Lyapunov spectrum of separated flows and its dependence on numerical discretization

P. Fernandez* and Q. Wang†
Department of Aeronautics and Astronautics, Massachusetts Institute of Technology,
77 Massachusetts Avenue, Cambridge, MA 02139, USA.
(Dated: December 23, 2016)

We investigate the Lyapunov spectrum of separated flows and their dependence on the numerical discretization. The chaotic flow around the NACA 0012 airfoil at low Reynolds number and large angle of attack is considered to that end, and t-, h- and p-refinement studies are performed to examine each effect separately. Numerical results show that the time discretization has a small impact on the dynamics of the system, whereas the spatial discretization can dramatically change them. In particular, the asymptotic Lyapunov spectrum for time refinement is achieved for CFL numbers as large as $\mathcal{O}(10^1 - 10^2)$, whereas the system continues to become more and more chaotic even for meshes that are much finer than the best practice for this type of flows.

arXiv:1612.07409v1 [physics.flu-dyn] 22 Dec 2016

CONTENTS

I. Introduction 1

II. Lyapunov analysis 1

III. Methodology 2
III.1. Numerical discretization 2
III.2. LE algorithm 2

IV. Numerical results 3
IV.1. Case description 3
IV.2. Effect of time resolution: t-refinement 3
IV.3. Effect of spatial resolution: h-refinement 3
IV.4. Effect of spatial accuracy order: p-refinement 5

V. Conclusions 5

Acknowledgments 6

References 6

I. INTRODUCTION

Lyapunov analysis is a powerful tool to characterize dynamical systems, and the first attempts to apply it to chaotic fluid flows date back from the '90s [7, 12, 13]. With the increase in computing power, Lyapunov analysis is gaining attention in the flow physics community [2, 17] as a promising approach for flow instability, vortex dynamics, and turbulence research. While the interest in flow physics lies in the Lyapunov spectrum of the actual flow, numerical algorithms compute the Lyapunov exponents of the finite-dimensional representation obtained after numerical discretization. It is therefore necessary to understand the impact of the spatial and temporal discretization on the resulting dynamics –e.g. is the spectrum of the discrete system that of the actual flow?

The Lyapunov spectrum of chaotic flow simulations also plays a key role in engineering. In particular, conventional sensitivity analysis methods break down for chaotic systems [8], and this compromises critical tasks such as flow control, design optimization, error estimation, data assimilation, and uncertainty quantification. While a number of sensitivity analysis methods have been proposed for chaotic systems [8, 9, 15, 16], they all come at a high computational cost. This is ultimately related to the positive portion of the Lyapunov spectrum, and the cost of each method is sensitive to different aspects of it –e.g. the cost of Non-Intrusive LSS [9] depends on the number of positive Lyapunov exponents, whereas the Ensemble Adjoint method [8] is postulated to be sensitive to the ratio of largest to smallest positive exponents [3]–. Hence, understanding the dynamics of chaotic flow simulations, and their dependence on numerical discretization, is necessary to estimate the cost and feasibility of chaotic sensitivity analysis methods.

In this paper, we investigate the Lyapunov spectrum of the separated flow around the NACA 0012 airfoil at Reynolds number $Re_\infty = 2,400$, Mach number $M_\infty = 0.2$, and angle of attack $\alpha = 20$ deg. Because the simulation is two-dimensional, the flow physics are different to those of three-dimensional flows. However, the moderate computational cost of this problem enable us to evaluate the impact of numerical discretization on the Lyapunov spectrum through a more comprehensive study than otherwise possible. In particular, the impact of temporal resolution (t-refinement), spatial resolution (h-refinement), and order of accuracy (p-refinement) are investigated.

The paper is structured as follows. In Section II, we present an overview of Lyapunov analysis. Section III describes the methodology to discretize the Navier-Stokes equations and perform Lyapunov analysis. Numerical results are then discussed in Section IV. Finally, we present some concluding remarks and future work in Section V.

II. LYAPUNOV ANALYSIS

The spatial discretization of the compressible Navier-Stokes equations yields a finite-dimensional, continuous-time, first-order dynamical system of the form

$$\frac{d\boldsymbol{u}_h}{dt} = \boldsymbol{f}_h(\boldsymbol{u}_h), \tag{1}$$

where $\boldsymbol{u}_h = \boldsymbol{u}_h(t)$ is an n-dimensional vector of state variables. In particular, $\boldsymbol{u}_h$ contains the conserved quantities

* pablof@mit.edu
† qiqi@mit.edu

(mass, momentum, total energy) at every grid point. Different meshes h and numerical schemes lead to different dimensions n and different dynamics $\boldsymbol{f}_h$.

For a system of the form (1), almost surely there exist scalars $\Lambda_h^1, \Lambda_h^2, ..., \Lambda_h^n \in \mathbb{R}$ such that, if $\Lambda_h^1 \neq \Lambda_h^2 \neq ... \neq \Lambda_h^n$, there exist vectors $\boldsymbol{\psi}_h^1(\boldsymbol{u}_h), \boldsymbol{\psi}_h^2(\boldsymbol{u}_h), ..., \boldsymbol{\psi}_h^n(\boldsymbol{u}_h) \in \mathbb{R}^n$ satisfying the evolution equation [11]

$$\begin{aligned}\frac{d}{dt}\boldsymbol{\psi}_h^j\big(\boldsymbol{u}_h(t)\big) =& \left.\frac{\partial \boldsymbol{f}_h}{\partial \boldsymbol{u}_h}\right|_{\boldsymbol{u}_h(t)} \boldsymbol{\psi}_h^j\big(\boldsymbol{u}_h(t)\big) \\ &- \Lambda_h^j\, \boldsymbol{\psi}_h^j\big(\boldsymbol{u}_h(t)\big), \quad j = 1, ..., n.\end{aligned} \tag{2}$$

$\boldsymbol{\psi}_h^j(\boldsymbol{u}_h)$ and Λ_h^j are the so-called covariant Lyapunov vectors (CLVs) and Lyapunov exponents (LEs), respectively. We note that the CLVs depend on the state $\boldsymbol{u}_h$, whereas the LEs are a property of the system independent of $\boldsymbol{u}_h$. Also, we shall asume that the Lyapunov exponents $\Lambda_h^1, ..., \Lambda_h^n$ are ordered from largest to smallest.

The intuitive interpretation of Lyapunov vectors and exponents is as follows: "Any infinitesimal perturbation $\delta\boldsymbol{u}_{h,0}$ in the direction $\boldsymbol{\psi}_h^j\big(\boldsymbol{u}(t_0)\big)$ at $t = t_0$ will remain in $\boldsymbol{\psi}_h^j\big(\boldsymbol{u}_h(t)\big)$ at all times $t \geq t_0$. Also, the magnitude of the perturbation increases or decreases at an average rate $\delta u_h(t) = \delta u_{h,0}\ \exp\big(\Lambda_h^j(t - t_0)\big)$". Hence, the magnitude and sign of the Lyapunov exponents characterize how infinitesimal perturbations to the system evolve over time. In particular, a system with $n^+ \geq 1$ positive exponents, $\Lambda_h^+ = \{\Lambda_h^1, ..., \Lambda_h^{n^+}\}$, displays chaotic dynamics. The positive exponent(s) are responsible for the "butterfly effect", a colloquial term to refer to the large sensitivity of chaotic systems to initial conditions. This is the case, for example, for turbulent flows as well as for many separated flows.

The numerical simulation of unsteady flows requires further discretizing Eq. (1) in time. This yields a discrete-time first-order map

$$\boldsymbol{u}_h^{(i+1)} = \boldsymbol{f}_{h,\Delta t}(\boldsymbol{u}_h^{(i)}), \tag{3}$$

where $\boldsymbol{u}_h^{(i)}$ denotes the solution at the end of the time step i. The particular form of $\boldsymbol{f}_{h,\Delta t}$ depends on $\boldsymbol{f}_h$, that is, on the spatial discretization, as well as on the time-integration scheme and the time-step size Δt. The discrete-time Lyapunov vectors $\boldsymbol{\psi}_{h,\Delta t}^j$ and exponents $\Lambda_{h,\Delta t}^j$ of $\boldsymbol{f}_{h,\Delta t}$ are defined in an analogous way to their continuous counterparts.

III. METHODOLOGY

III.1. Numerical discretization

High-order Hybridizable Discontinuous Galerkin (HDG) and diagonally implicit Runge-Kutta (DIRK) methods are used for the spatial and temporal discretization of the compressible Navier-Stokes equations, respectively [6]. The HDG method, as a discontinuous Galerkin method, allows for a systematic study of the effect of the accuracy order on the Lyapunov spectrum via p-refinement.

III.2. LE algorithm

A non-intrusive version of the algorithm by Benettin *et al.* [1] is used to compute the $p \leq n$ leading Lyapunov exponents.

Original algorithm. The original procedure in [1] is summarized in Algorithm 1. If the time integrals in Steps No. 5 and 6 of the algorithm are computed exactly, an estimator of the p leading continuous-time LEs $\hat{\Lambda}_h$ of $\boldsymbol{f}_h$ are obtained. If the time integrals are approximated using a numerical method, as it is the case in practice, the algorithm computes an estimator of the p leading discrete-time Lyapunov exponents $\hat{\Lambda}_{h,\Delta t}$ of $\boldsymbol{f}_{h,\Delta t}$.

Data: Initial condition $\boldsymbol{u}_{h,0}$, number of exponents to compute p, length of each time segment T_s, and number of time segments K.
Result: Estimators of the p largest LEs $\hat{\Lambda}_h^j,\ j = 1, ..., p$.
1. Set $t_0 = 0$ and $\boldsymbol{u}_h(t_0) = \boldsymbol{u}_{h,0}$.
2. Compute an $n \times p$ random matrix

$$V^{\langle 0\rangle} \sim \big[\mathcal{U}(0,1)\big]^{n\times p}.$$

3. Compute the reduced QR decomposition

$$Q^{\langle 0\rangle} R^{\langle 0\rangle} = V^{\langle 0\rangle}.$$

for $i = 1$ **to** K **do**
4. Set $t_i = t_{i-1} + T_s$.
5. Time integrate the dynamical system (1) from t_{i-1} to t_i using the initial condition $\boldsymbol{u}_h^{\langle i-1\rangle} = \boldsymbol{u}_h(t_{i-1})$.
6. Time integrate the tangent equation (4) from t_{i-1} to t_i for each of the p initial conditions given by the columns of $Q^{\langle i-1\rangle}$ using the reference trajectory $\boldsymbol{u}_h$ computed in Step No. 5,

$$\frac{d\boldsymbol{v}_j}{dt} = \left.\frac{\partial \boldsymbol{f}_h}{\partial \boldsymbol{u}_h}\right|_{\boldsymbol{u}_h(t)} \boldsymbol{v}_j, \qquad \boldsymbol{v}_j(t_{i-1}) = \boldsymbol{q}_j^{\langle i-1\rangle}, \tag{4}$$

for $j = 1, ..., p$, and set $\boldsymbol{v}_j^{\langle i\rangle} = \boldsymbol{v}_j(t_i)$. Here, $\boldsymbol{q}_j^{\langle i\rangle}$ and $\boldsymbol{v}_j^{\langle i\rangle}$ denote the j-th column of $Q^{\langle i\rangle}$ and $V^{\langle i\rangle}$.
7. Compute the reduced QR decomposition

$$Q^{\langle i\rangle} R^{\langle i\rangle} = V^{\langle i\rangle}.$$

end
8. Compute

$$\hat{\Lambda}_h^j = \frac{1}{t_K - t_0} \sum_{i=1}^{K} \log |R_{jj}^{\langle i\rangle}|. \tag{5}$$

Algorithm 1: Original algorithm by Benettin *et al.* [1] to compute LEs. The superscript $\langle i\rangle$ denotes the solution at the end of the time segment i.

Modified algorithm. Since the original algorithm requires the integration of the tangent equation (4) in Step No. 6, it cannot be used with existing computational fluid dynamics (CFD) solvers without modification of the source code. In the

spirit of making the algorithm non-intrusive, we approximate the tangent map (4) by finite differences. In particular, let $\boldsymbol{u}_h^{\langle i \rangle} = \boldsymbol{g}_{h,\Delta t}(\boldsymbol{u}_h^{\langle i-1 \rangle};\, T_s)$ denote the Navier-Stokes map over the time segment $[t_{i-1}, t_i]$ of length T_s computed by a CFD code starting from the initial condition $\boldsymbol{u}_h^{\langle i-1 \rangle}$ at t_{i-1}. We then replace Step No. 6 in Algorithm 1 by

$$\begin{aligned} \boldsymbol{v}_j^{\langle i \rangle} \approx & \frac{1}{\epsilon}\Big[\boldsymbol{g}_{h,\Delta t}\big(\boldsymbol{u}_h(t_{i-1}) + \epsilon\, \boldsymbol{q}_j^{\langle i-1 \rangle};\, T_s\big) \\ & - \boldsymbol{g}_{h,\Delta t}\big(\boldsymbol{u}_h(t_{i-1});\, T_s\big)\Big], \qquad j = 1, ..., p, \end{aligned} \tag{6}$$

Here, T_s is small enough such that $|\boldsymbol{g}_{h,\Delta t}\big(\boldsymbol{u}_h(t_{i-1}) + \epsilon\, \boldsymbol{q}_j^{\langle i-1 \rangle};\, T_s\big) - \boldsymbol{g}_{h,\Delta t}\big(\boldsymbol{u}_h(t_{i-1});\, T_s\big)| \ll 1$, and ϵ satisfies $\epsilon_{tol} \ll \epsilon \ll 1$, where ϵ_{tol} denotes the tolerance of the solver for the nonlinear system of equations arising from the DIRK discretization.

IV. NUMERICAL RESULTS

IV.1. Case description

We consider the two-dimensional, separated flow around the NACA 0012 airfoil at Reynolds number $Re_\infty = u_\infty c/\nu = 2400$, Mach number $M_\infty = u_\infty/a_\infty = 0.2$, and angle of attack $\alpha = 20$ deg. Here, u_∞, a_∞, ν and c denote the freestream velocity, freestream speed of sound, kinematic viscosity, and airfoil chord, respectively. The computational domain is partitioned using isoparametric triangular elements, and the outer boundary is located 10 chords away from the airfoil. A non-slip, adiabatic wall boundary condition is imposed on the airfoil surface, and a characteristics-based, non-reflecting boundary condition is used on the outer boundary.

IV.2. Effect of time resolution: t-refinement

We analyze the effect of the time-step size on the Lyapunov spectrum of the discrete system $\boldsymbol{f}_{h,\Delta t}$. In particular, the continuous-time system $\boldsymbol{f}_h$ associated to a fourth-order discretization (i.e. $p = 3$) with 115,200 degrees of freedom (DOFs) is time-integrated using the time steps $\Delta t = (0.0400,\ 0.0200,\ 0.0100,\ 0.0050,\ 0.0025)\ c/a_\infty$. These correspond to maximum CFL numbers of 59.94, 29.97, 14.98, 7.49, and 3.75. We emphasize that the time-step size affects the discrete-time map $\boldsymbol{f}_{h,\Delta t}$ but does not change $\boldsymbol{f}_h$.

Figure 1 shows 90% confidence intervals of the six leading Lyapunov exponents for the time-step sizes considered. The confidence intervals are computed from the sample variance of $\log|R_{jj}^{\langle i \rangle}|$ in Eq. (5) and the Central Limit Theorem. From this figure, the time-step size in the range considered does not have a significant impact on the leading exponents of $\boldsymbol{f}_{h,\Delta t}$. First, this gives us confidence that the time steps considered suffice for the discrete-time Lyapunov exponents to approximate those of the continuous-time system, i.e. $\Lambda_{h,\Delta t}^j \approx \Lambda_h^j$. For this reason, we shall refer to $\boldsymbol{f}_h$ and Λ_h, instead of $\boldsymbol{f}_{h,\Delta t}$ and $\Lambda_{h,\Delta t}$, in the remainder of the paper. Second, the asymptotic spectrum of the discrete-time map as $\Delta t \to 0$ is achieved with CFL numbers $\mathcal{O}(10 - 100)$ that are larger than those used in engineering practice. This is attributed to these time-step sizes being sufficiently small to resolve the vortical structures that are responsible for the chaotic dynamics. However, if $\Delta t \gg h_{sep}/u_\infty$, where h_{sep} denotes the element size in the separated region, the discrete-time map might not accurately reproduce the continuous-time system, and therefore $\Lambda_{h,\Delta t}^j \not\approx \Lambda_h^j$. This has indeed been observed in [10] for the numerical integration of stiff ODEs with inadequate time steps.

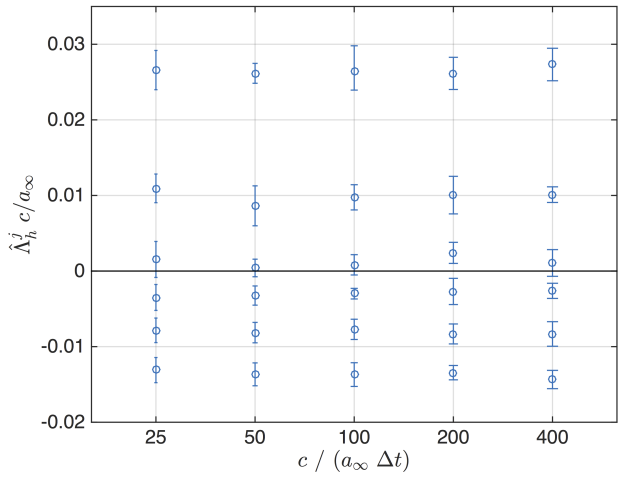

FIG. 1: 90% confidence intervals of the six leading Lyapunov exponents in the t-refinement study.

IV.3. Effect of spatial resolution: h-refinement

In this section, we examine the effect of the spatial resolution on the number and magnitude of positive exponents. To that end, the Lyapunov spectrum is computed for eleven O-meshes, each of them $2^{1/3}$ times finer per direction than the previous one. The number of DOFs uniformly increases in logarithmic scale from 7,200 (mesh No. 1) to 726,240 (mesh No. 11). Meshes No. 1 and 11 are shown in Fig. 2. We note that mesh No. 1 is intended to be pathologically coarse to analyze how the system behaves for very under-resolved meshes.

The discretization scheme and time-step size are kept constant to analyze the effect of spatial resolution only. In particular, fourth-order ($p = 3$) HDG and third-order DIRK methods are used for the spatial and temporal discretization, respectively, and the time-size is set to $\Delta t = 0.05\ c/a_\infty$. A run up time of $2,000\ c/a_\infty$ is used to drive the system to the attractor, and the LE algorithm is then applied for $K = 12,000$ time segments each of length $T_s = c/a_\infty$. Figure 3 shows the 14 leading LEs for the discretizations considered, whereas Table I collects the Kaplan-Yorke dimension D_{KY} [4] of the h-family of attractors. From these results, several remarks follow:

- The magnitude of the leading LE and the number of positive exponents increase above a spatial resolution

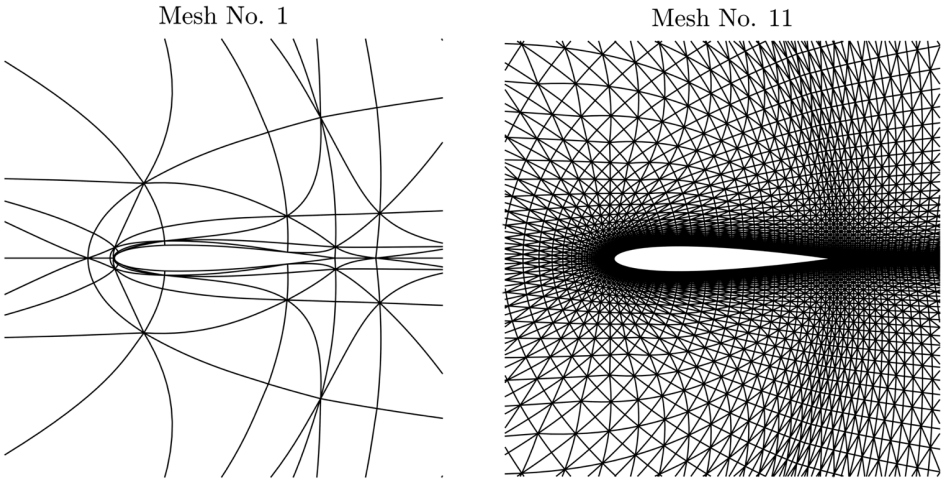

FIG. 2: Coarsest and finest high-order meshes used in the h-refinement study.

threshold h^*, corresponding to mesh No. 5. That is, the discrete system becomes more chaotic above this resolution as the mesh is refined. This is attributed to the fact that more vortical structures, which are responsible for the chaotic dynamics of the flow, are resolved as the numerical resolution is increased.

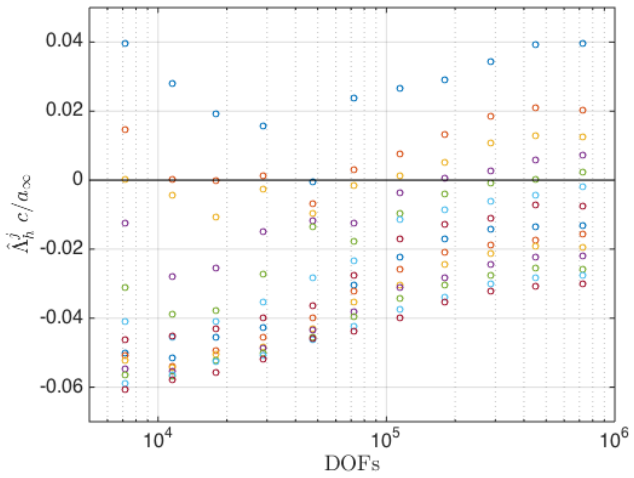

FIG. 3: 14 leading Lyapunov exponents of the h-family of dynamical systems.

- Below the resolution threshold h^*, the discrete system poorly reproduces the dynamics of the continuous system, and this results in spurious dynamics. Here, spurious periodicity and chaoticity are observed. (No discretization results in stable dynamics.) Discretization No. 5, for example, has no positive LEs and is periodic. A time refinement study confirmed that the continuous-time system associated to this discretization $\boldsymbol{f}_{h_5}$ –and not only the discrete-time map $\boldsymbol{f}_{h_5,\Delta t}$– is indeed periodic. Hence, for the h-family of discrete dynamical systems considered here, a periodic orbit bifurcates into strange attractors above and below $\sim h_5$. We hypothesize this is a numerical artifact and therefore discretization dependent. For example, spurious chaoticity may not be observed in methods with high numerical dissipation, such as first-order schemes. For these methods, stable dynamics with a fixed point could be obtained instead with a very coarse mesh.

- An approximately zero exponent $\Lambda_h \approx 0$ is present in all discretizations. Theoretical results show that $\Lambda_h = 0$ with $\boldsymbol{\psi}_h = \boldsymbol{f}_h(\boldsymbol{u}_h)$ for periodic and chaotic systems. This is expected to be such a exponent, and the error is attributed to the variance of the estimator and, to a lessen extent, the approximation $\Lambda_{h,\Delta t} \approx \Lambda_h$.

- The positive Lyapunov exponents are created from bifurcations of the $\Lambda_h = 0$ exponent at discrete mesh resolutions.

The trace of drag c_d and lift c_l coefficients over a time interval $\Delta t = 20,000\; c/a_\infty$ is shown in Fig. 4, where the dots are colored by probability density function (PDF) in (c_d, c_l) space. Despite the chaotic dynamics of discretization No. 7, we note that the PDF resembles the periodic trace of mesh No. 5. The period for this discretization, $T_5 \approx 75.70\; c/a_\infty$, is four times the dominant vortex shedding period. The Strouhal number for the h-family of discretizations are collected in Table I.

Next, we investigate if an asymptotic Lyapunov spectrum is achieved with the numerical resolutions that can be afforded in engineering practice. To this end, we consider a fourth-order discretization with 2,880,000 degrees of freedom. This is vastly more than the best-practice meshes for this type of flows. The 90% confidence interval of the leading Lyapunov exponent for this discretization is $\Lambda_h^1\; c/a_\infty = 0.04732 \pm 0.005275$. Hence, the system continues to become more chaotic even for this discretization.

While an asymptotic Lyapunov spectrum as $h \to 0$ was obtained for simpler partial differential equations in other studies [14], this result shows that such an asymptotic spectrum –if exists– is difficult to achieve in practice even for simple flows. This is in contrast to the results for the time discretization in Section IV.2.

Discretization No.	1	2	3	4	5	6	7	8	9	10	11
St	0.24	0.23	0.26	0.24	0.26	0.26	0.26	0.26	0.26	0.26	0.26
D_{KY}	4.73	2.14	2.68	2.01	1.00	3.29	5.37	7.72	8.27	9.19	10.90

TABLE I: Strouhal number St and Kaplan-Yorke attractor dimension D_{KY} [4] of the h-family of discretizations.

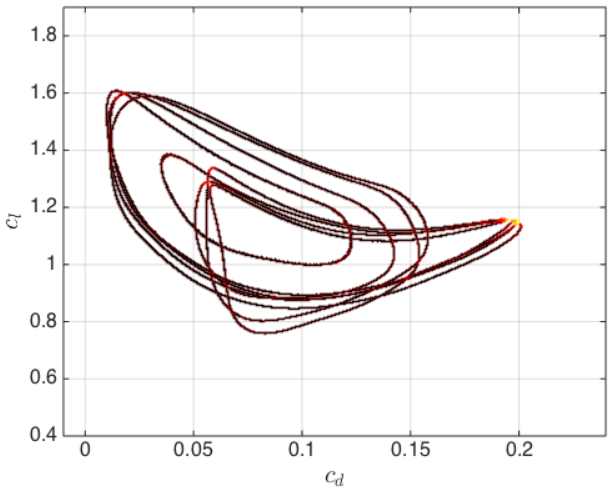

(a) Mesh No. 5

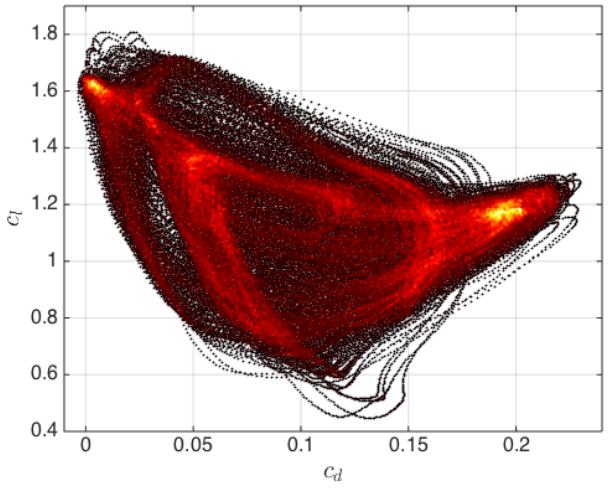

(b) Mesh No. 7

FIG. 4: (c_d, c_l) trace over a time interval $\Delta t = 20,000\ c/a_\infty$. The dots are colored by probability density function in (c_d, c_l) space.

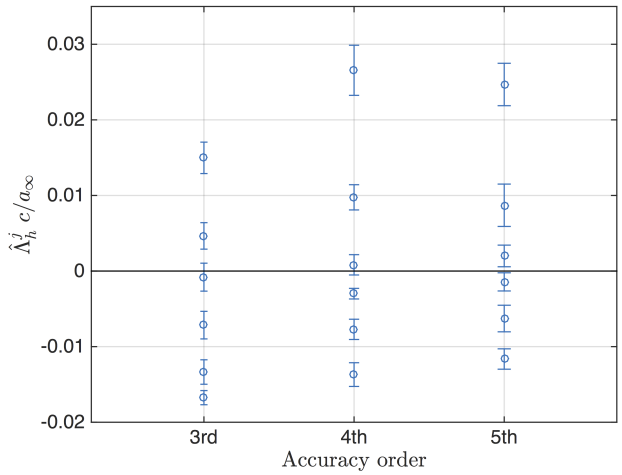

FIG. 5: 90% confidence intervals of the six leading Lyapunov exponents in the p-refinement study.

IV.4. Effect of spatial accuracy order: p-refinement

Finally, we investigate the effect of the accuracy order of the spatial discretization on the dynamics of $\boldsymbol{f}_h$. To this end, third-, fourth-, and fifth-order HDG schemes (i.e. $(p = \{2, 3, 4\})$ are considered. The DIRK(3,3) method with $\Delta t = 0.05\ c/a_\infty$ is used for the time integration, and the number of degrees of freedom is 115,200 in all cases. This corresponds to resolution No. 7 in the h-refinement study.

Figure 5 shows 90% confidence intervals of the six leading Lyapunov exponents for the accuracy orders considered. From this figure, the negative LEs get closer to zero, that is, perturbations along stable directions decay more slowly, as the accuracy order increases. This is attributed to the lower numerical dissipation of high-order methods. Also, the fourth- and fifth-order methods lead to larger positive exponents than the third-order scheme –i.e. perturbations along unstable directions get more rapidly amplified. The 90% condiference intervals for the fourth- and fifth-order discretizations overlap and it is not possible to conclude which scheme results in more chaotic dynamics.

V. CONCLUSIONS

We investigated the impact of the numerical discretization on the Lyapunov spectrum of chaotic, separated flow simulations. Numerical results showed that the time discretization has a small effect on the Lyapunov spectrum for the time-step sizes typically used in CFD practice. In particular, the asymptotic spectrum as $\Delta t \to 0$ was achieved for CFL numbers $\mathcal{O}(10^1 - 10^2)$. The spatial discretization, however, was shown to dramatically change the dynamics of the system. First, the discretized system poorly reproduced the dynamics of the flow, and spurious dynamics were observed, below some spatial resolution threshold. Second, the discrete system continued to become more and more chaotic even with finer meshes than the best practice for this type of flows. This indicates that the asymptotic Lyapunov spectrum as $h \to 0$, if exists, is difficult to achieve in practice even for simple flows.

ACKNOWLEDGMENTS

The authors acknowledge AFOSR Award 14RT0138 under Dr. Fariba Fahroo and Dr. Jeanluc Cambrier, and Stanford CTR Summer Program 2016. The first author also thanks "la Caixa" Foundation for the Graduate Studies Fellowship that support his work.

[1] G. Benettin, L. Galgani, A. Giorgilli, J. Strelcyn, Lyapunov characteristic exponents for smooth dynamical systems and for Hamiltonian systems; a method for computing all of them. Part 2: Numerical application, Meccanica 15 (1) (1980) 21–30.

[2] P.J. Blonigan, P. Fernandez, S.M. Murman, Q. Wang, G. Rigas, L. Magri, Towards a chaotic adjoint for LES, Proceedings of the Center for Turbulence Research Summer Program 2016, To appear.

[3] N. Chandramoorthy, Q. Wang, An Analysis of the Ensemble Adjoint Approach toSensitivity Analysis in Chaotic Systems, In preparation for sumission.

[4] J.-P. Eckmann, D. Ruelle, Ergodic theory of chaos and strange attractors, Reviews of Modern Physics 57 (3) (1985) 617–656.

[5] J.D. Farmer, J.J. Sidorowich, Optimal shadowing and noise reduction, Physica D, 47 (1991) 373–392.

[6] P. Fernandez, N.C. Nguyen, X. Roca, J. Peraire, Implicit large-eddy simulation of compressible flows using the Interior Embedded Discontinuous Galerkin method, In: 54th AIAA Aerospace Sciences Meeting, San Diego, USA, 2016.

[7] L. Keefe, P. Moin, J. Kim, The dimension of attractors underlying periodic turbulent Poiseuille flow, J. Fluid Mech. 242 (1992) 1–29.

[8] D.J. Lea, M.R. Allen, T.W. Haine, Sensitivity analysis of the climate of a chaotic system, Tellus A 52 (2000) 523–532.

[9] A. Ni, Q. Wang, Sensitivity analysis on chaotic dynamical system by Non-Intrusive Least Square Shadowing (NILSS), to be submitted to Journal of Computational Physics, arXiv: 1611.00880

[10] E. Özkaya, N.R. Gauger, A. Nemili, Chaotic Behavior of Stiff ODEs and Their Derivatives: An Illustrative Example, arXiv:1610.03358 (2016).

[11] V.I. Oseledets, Multiplicative ergodic theorem: Characteristic Lyapunov exponents of dynamical systems, Trudy MMO 19 (1968) 179–210.

[12] T. Pulliam, J. Vastano, Transition to chaos in an open unforced 2D flow, J. Comput. Phys. 105 (1993) 133–149.

[13] L. Sirovich, A. Deane, A computational study of Rayleigh-Benard convection. Part 2. Dimension considerations, J. Fluid Mech. 222 (1991) 251–266.

[14] K.A. Takeuchi, H-l Yang, F. Ginelli, G. Radons, H. Chaté, Hyperbolic decoupling of tangent space and effective dimension of dissipative systems, Physical Review E 84 (2011) 046214.

[15] J. Thuburn, Climate sensitivities via a FokkerPlanck adjoint approach, Quarterly Journal of the Royal Meteorological Society 131 (605) (2005) 73–92.

[16] Q. Wang, R. Hui, P. Blonigan, Least squares shadowing sensitivity analysis of chaotic limit cycle oscillations, J. Comput. Phys. 267 (2014) 210–224.

[17] M. Xu, M.R. Paul, Covariant Lyapunov vectors of chaotic Rayleigh-Bénard convection, Physical Review E 93 (2016) 062208.